Cavitation during Isothermal Crystallization of Isotactic Polypropylene

R. NOWACKI, J. KOLASINSKA, E. PIORKOWSKA

Centre of Molecular and Macromolecular Studies, Polish Academy of Sciences, 90-363 Lodz, Poland

Received 14 February 2000; accepted 24 May 2000

ABSTRACT: Cavitation during isothermal crystallization of thin films of isotactic polypropylene was investigated systematically by light microscopy. Cavitation results from the negative pressure buildup due to density change during crystallization in the pockets of melts occluded by impinging spherulites. The morphology of such areas was also studied by SEM. The value of the negative pressure at the moment of cavitation was calculated from the drop of the spherulite growth rate. It was shown that the process of cavitation and the value of the negative pressure causing cavitation depend on the crystallization temperature. © 2001 John Wiley & Sons, Inc. J Appl Polym Sci 79: 2439–2448, 2001

Key words: cavitation; negative pressure; isotactic polypropylene; crystallization

INTRODUCTION

In the course of crystallization, the impinging spherulites occlude pockets of the melt, hindering further inflow of the melt.[1,2] Hence, the crystallization there is accompanied by a buildup of negative pressure due to a lower specific volume of a solid. In thin films, the negative pressure arises only during crystallization between two plates. In thin films crystallized with a free surface, the thinning of a sample occurs within pockets instead of the negative pressure buildup. The negative pressure causes cavitation in the melt confined between spherulites which releases the pressure in the melt but results in voids within the spherulitic structure.[1–5] The cavitation occurring preferably at the solid–liquid interface in isotactic polypropylene was observed in ref. 5. Local stresses or holes weaken the material; hence, the areas occluded during crystallization constitute "weak spots" of the spherulitic structure.

The negative pressure in weak spots lowers the equilibrium melting temperature, T_m^0, and, hence, decreases locally the undercooling. It was demonstrated in ref. 6 that negative pressure in weak spots causes a significant decrease of the growth rate of isotactic polypropylene spherulites; hence, the decrease of the growth rate can be used for the determination of the negative pressure level. Negative pressure results also in the crystallization of thicker lamellae which show a higher melting temperature.[6–8] The reduced cross-hatching in isotactic polypropylene spherulites crystallized under negative pressure was also observed.[9] The intense nucleation of β spherulites after cavitation inside weak spots was noticed first in ref. 10 and later in ref. 11. At an elevated crystallization temperature, the fractures along the interspherulitic boundaries were observed instead of cavitation.[3,4,11]

It was shown in refs. 12 and 13 that cavitation within weak spots was accompanied by emission of ultrasound which depends on the crystalliza-

Correspondence to: E. Piorkowska.

Contract grant sponsor: State Committee for Scientific Research, Poland; contract grant number: 7 T08E 016 12.

Journal of Applied Polymer Science, Vol. 79, 2439–2448 (2001)

tion temperature and can be suppressed by addition of a nucleating agent to a polymer. The gas pressure inside the cavitation bubbles immediately after crystallization was found to be much lower than was the atmospheric pressure.[2]

In the present work, the cavitation in isotactic polypropylene crystallized isothermally was systematically studied as a function of the crystallization temperature. The negative pressure values at the moment of cavitation were estimated from the decrease of spherulite growth rate in relation to the crystallization temperature.

EXPERIMENTAL

Isotactic polypropylene (iPP), a Polysciences product (Warrington, PA) having M_n = 17,000 and M_w = 220,000, in the form of thin films obtained by compression molding, was studied. The films were placed between two circular coverglasses and then melted at 220°C and the melt annealed for 3 min and cooled at the rate 10 K/min to the crystallization temperature (T_c) chosen from the range 124–140°C. The samples were isothermally crystallized and cooled to room temperature at a rate of 5 K/min. The entire procedure was performed under a flow of pure nitrogen, in a Linkam hot-stage TMS 92 mounted on a light microscope. The precision of the temperature control was 0.1 K, while the uniformity of the thickness of each film, around 30 μm, was ensured by a ring-shaped layer of aluminum foil at the edges of the glasses. The samples were monitored by a light microscope during crystallization and cooling. The microscope was connected to a closed-circuit TV (CCTV) camera, CCTV display, VHS video recorder, and computer equipped with a frame grabber card. Several samples were crystallized and studied for each crystallization temperature. The time was measured using a Linkam Video Text Overlay VTO 232 with the precision of 0.1 s. The images were recorded at the rate 1 per 0.04 s.

The spherulite growth rate, G, for iPP was determined from the change of the position of the crystallization front in successive time intervals for T_c up to 141°C. The growth rate, G, of isolated spherulites was measured to obtain information about the possible fractionation of low molecular weight and atactic fractions and the segregation of additives. The values of G measured at the beginning of crystallization were used to construct the temperature dependence of G. G was also measured within weak spots until the end of crystallization there. Care was taken to measure G in short time intervals just before cavitation in weak spots. The surface area of the uncrystallized melt inside the weak spots was measured beginning with the moment of their formation.

After cooling to room temperature, the upper glass was removed from the samples. Then, the samples were evaporated with gold and examined under a scanning electron microscope.

The microscopic glasses, manufactured by Chance Proper Ltd., Great Britain, were washed in ethanol before use. Also, glasses cleaned in a mixture of sulfuric acid and potassium dichromate and later washed in distilled water in an ultrasonic bath were used to determine the possible influence of the cleaning procedure on the cavitation phenomena. We have to note here that both procedures for cleaning the glasses led to similar cavitation behavior.

RESULTS

Light Microscopy

The cavitation was observed in occluded pockets of the iPP melt during isothermal crystallization at T_c from 124 to 139°C. Figure 1 shows a set of micrographs illustrating the crystallization in a weak spot at 128°C. The occlusion of the melt by impinging spherulites hinders the influx of the melt to the weak spot. After some accumulation of melt deficiency, cavitation occurs, which is accompanied by a negative pressure release in the melt. Cavities of various sizes are formed inside the same weak spot in many places simultaneously (i.e., within a 0.04-s interval) . Large bubbles of several micrometers' diameters or more are formed at the interface melt-crystallizing front and less frequently in the melt. Very often, those large cavities appear in the vicinity of interspherulitic boundaries. At lower T_c, the large cavities predominantly appear at the crystallization front. With increasing T_c, their number decreases, so the relative number of cavities inside a melt increases. In Figure 2, cavitation bubbles at the crystallization front at 130°C are shown at the moment of cavitation and 0.1 s later. While at the first moment they are rather poorly discernible, except for the largest one they become clearly visible after 0.1 s.

At the moment when large bubbles are formed, a dark line appears where the crystallizing front

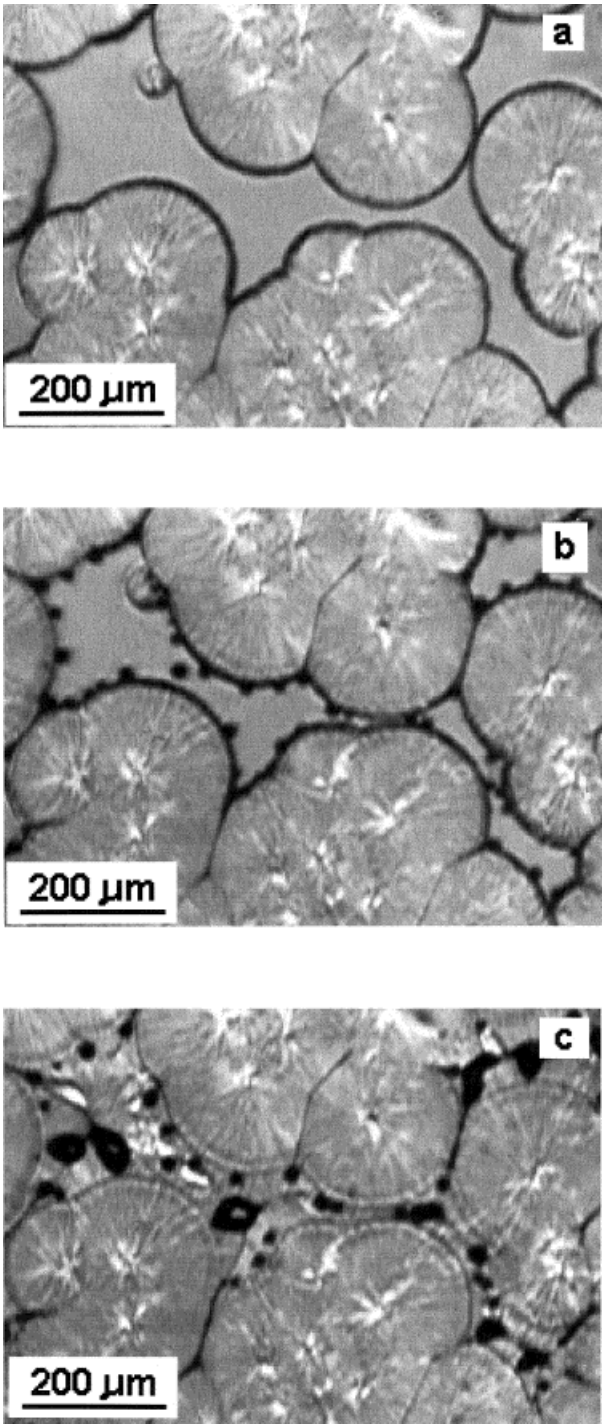

Figure 1 Crystallization in weak spot at 128°C in iPP film between microscopic glasses: (a) occlusion of melt by spherulites; (b) cavitation; (c) final structure.

adheres to the glass. Due to the curvature of the spherulite surfaces in 30-μm-thick film, it was possible sometimes to distinguish dark lines at the upper and lower coverglasses. They were

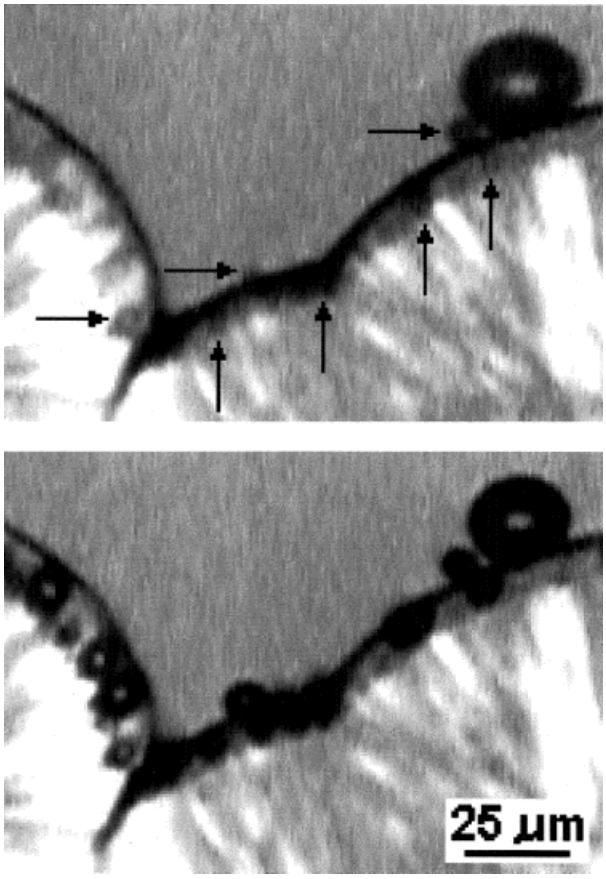

Figure 2 Micrographs of iPP spherulite–melt interphase at 130°C: (upper) at the moment of cavitation; (lower) 0.1 s later. Arrows in upper micrograph indicate cavitation bubbles.

identified as rows of small bubbles of diameters not exceeding 1–2 μm (Fig. 3). No such bubbles were found at those parts of the crystallizing front which does not adhere to the glasses. The forma-

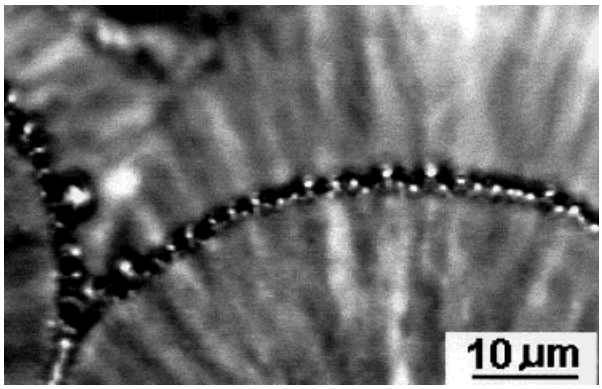

Figure 3 Details of cavities formed at 128°C at iPP spherulite–melt interphase near upper glass.

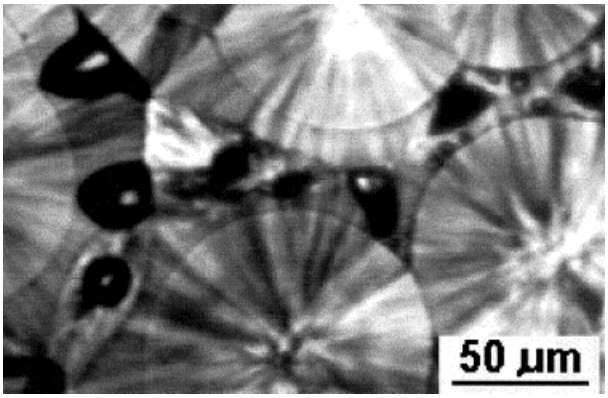

Figure 4 Weak spot after the completion of iPP film crystallization at 124°C.

tion of rows of small bubbles depends on the T_c. With increase of the T_c, they are visible less frequently; at 134°C and higher T_c, the weak spots without such dark lines composed of numerous small cavities are also observed. It was noticed, especially at lower T_c, where the weak spots are close to each other, that neighboring weak spots often cavitate nearly at the same time, that is, within the time interval of 0.04–0.2 s.

Figure 4 shows a weak spot after the completion of crystallization. Usually, new spherulites inside a weak spot are visible, very often nucleated on cavitation bubbles, with many β-form spherulites among them. While β spherulites are nucleated exclusively on the cavitation bubbles, the α spherulites with and without bubbles in the centers are observed. The cavitation bubbles either are occluded by growing spherulites or they enlarge in the course of further crystallization. Very rarely, the cavitation bubbles diminish and disappear just after their formation.

Simultaneously with the cavitation, a fracture of the polymer along the interspherulitic boundaries is observed. This phenomenon depends on the T_c; it begins to appear at 124°C but it is rather a marginal effect until 130°C. With the elevation of the T_c, the fracture fissures become longer and more numerous. Observations carried out at higher magnification reveal narrow channels of melt between spherulites surrounding weak spots. The voids, having diameters not exceeding several micrometers, appear in these narrow channels of the melt (Fig. 5) simultaneously with the formation of bubbles inside the melt and along the crystallizing front within the weak spots. The voids enlarge, elongate, and merge during further crystallization. The movement of the bubbles in the direction opposite to a weak spot is also observed. Sometimes, inhabited spaces by voids along the interspherulitic boundaries elongate slightly during cooling. In samples crystallized at 132°C and higher T_c, the radial fissures of spherulites propagating toward spherulite centers are noticed. The detailed observations reveal also the cavitational mechanism. The phenomenon intensifies with increase of the T_c.

Besides cavitating weak spots, weak spots which do not cavitate are also observed. The number of weak spots cavitating during isothermal crystallization diminish with increase of the crystallization temperature. Starting from 132°C, no cavitating weak spot can be found inside the observed area of 3 mm^2. Weak spots noncavitating during isothermal crystallization at 132°C and higher T_c fracture often during cooling, usually below 100°C, rarely in the range of 100–110°C. Fracture fissures appear along interspherulitic boundaries and along spherulite radii. Figure 6 shows a set of micrographs of this phenomenon

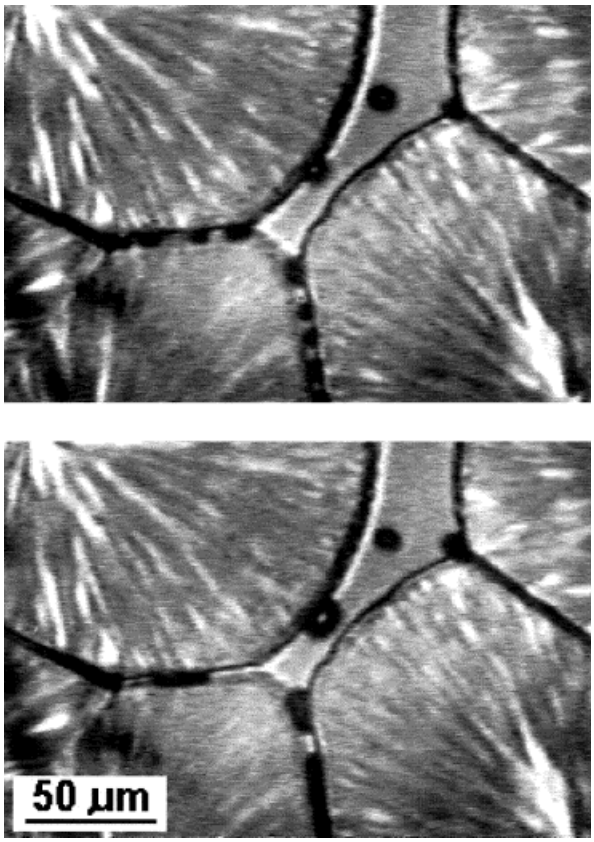

Figure 5 Cavitation along boundaries between spherulites forming a weak spot during crystallization at 130°C in iPP film between microscopic glasses.

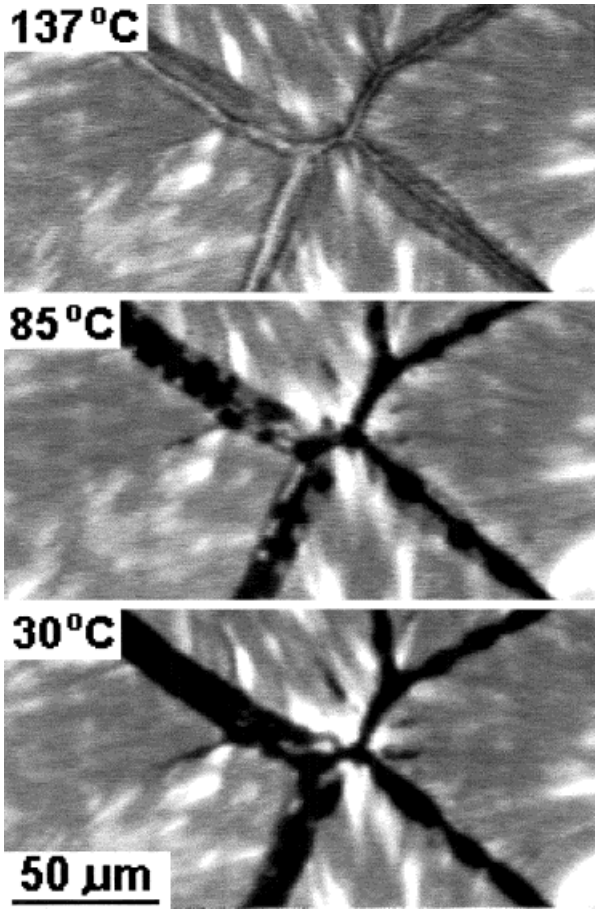

Figure 6 Cavitation along boundaries between iPP spherulites during cooling at the rate of 5 K/min after isothermal crystallization at 137°C.

within the weak spot in a sample crystallized at 137°C. At 137°C, a layer of a molten polymer above the spherulite boundaries is visible, which does not crystallize at isothermal conditions at this temperature. During cooling, the cavitation occurs at 85°C. The cavities enlarge and merge during further cooling. The molten polymer layer crystallizes, and at 30°C, it is no longer recognizable. The voids emerging at the spherulite boundaries are also seen where a layer of molten polymer was not so clearly discernible under a light microscope. It should be mentioned that cavitation along boundaries occurs at different temperatures at different places of the same sample. The annealing of samples at the crystallization temperature or at a lower temperature (e.g., 1.5 h at 115°C), where crystallization of iPP is fast, does not affect this phenomenon. It should be mentioned that during cooling no new fractures appear inside the weak spots which cavitated in the course of isothermal crystallization.

During crystallization at 140°C, the cavitation within weak spots was not observed; however, numerous small voids appeared along the interspherulitic boundaries during cooling. Cavitation along the spherulites radii was also visible.

The voids formed during crystallization and cooling disappear when samples are melted. After storage for several days at room temperature, the samples studied in a light microscope revealed additional fractures along the spherulite boundaries and also within weak spots.

Scanning Electron Microscopy (SEM)

SEM studies revealed voids in the iPP samples. They are visible between the spherulites, along the interspherulitic boundaries, and also along the spherulite radii. Their features seen to conform to those observed under the light microscope. Figure 7 shows an SEM micrograph of a weak spot in the sample crystallized at 128°C. The white areas visible in the SEM micrographs correspond to bubbles in a polymer beneath the surface of the sample. During exposure to an electron beam, they tend to open to a sample surface due to irradiation damage. The small bubbles are arranged in chains corresponding to those visible under a light microscope. Figure 8 illustrates the morphology of the large holes formed between the spherulites in a weak spot, while in Figure 9, voids along the interspherulitic boundary and along the spherulite radii are visible in the sample crystallized at 132°C.

Growth Rate and Surface-Area Measurements

The typical time dependence of the spherulite growth rate, G, in a cavitating weak spot at 130°C

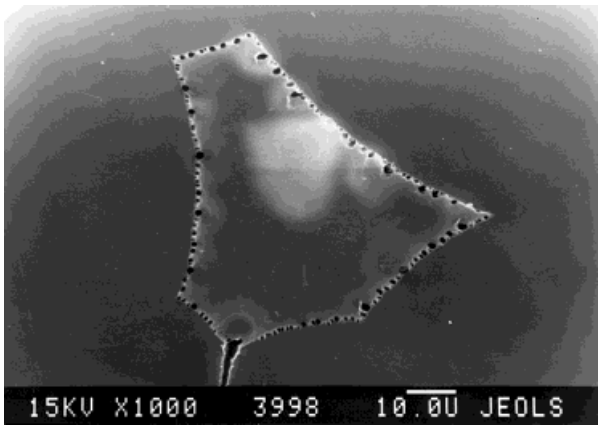

Figure 7 SEM micrograph of the weak spot in iPP film crystallized at 128°C.

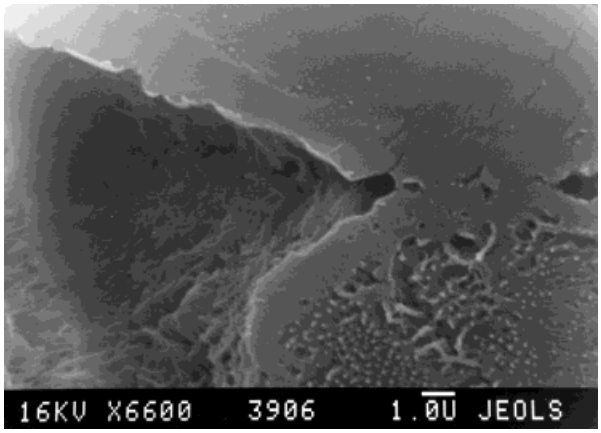

Figure 8 SEM micrograph of large hole between spherulites in iPP film crystallized at 132°C.

is shown in Figure 10. From the moment of occlusion of the melt by the spherulites, G decreases due to negative pressure buildup until cavitation occurs, releasing the pressure in the melt; then, G increases instantaneously. At 130°C, the decrease of G with time was measured as being the same for all spherulites inside the same weak spot, while it can be different for a single spherulite taking part in two separate weak spots.

The iPP spherulite growth rate, G, depends on crystallization temperature, T_c, in a well-known way[14]:

$$G = G_0 \exp\{-U[R(T_c - T_\infty)]^{-1}\} \times \exp\{-K_g[T_c(T_m^0 - T_c)]^{-1}\} \quad (1)$$

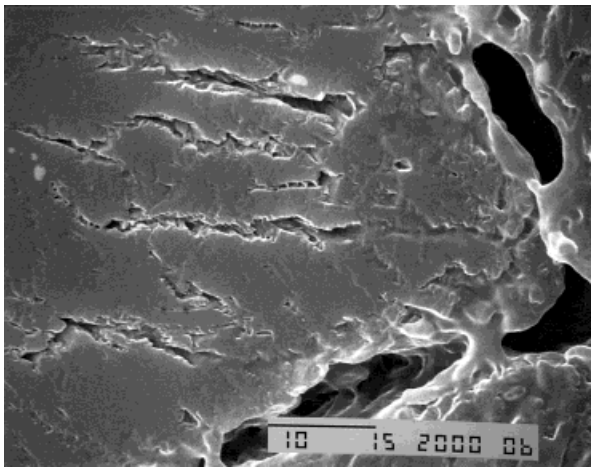

Figure 9 SEM micrograph of voids along interspherulitic boundary and along spherulite radii in iPP film crystallized at 132°C. The scale bar denotes 10 μm.

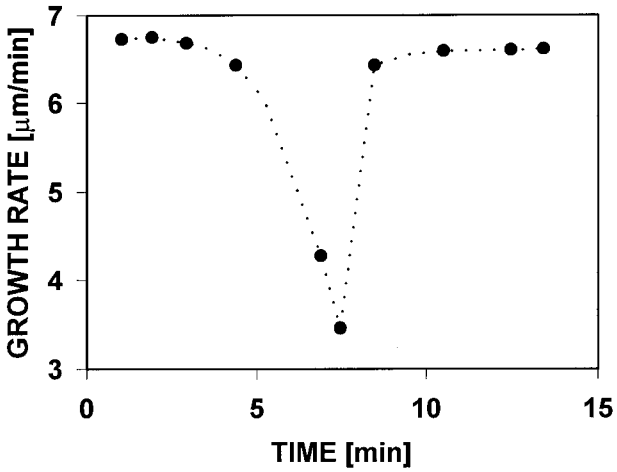

Figure 10 Time dependence of iPP spherulite growth rate in a cavitating weak spot at 130°C from the moment of occlusion of the melt by spherulites until the end of crystallization there.

where $U = 1500$ cal mol^{-1}, $T_\infty = 231.2$ K, and $T_m^0 = 458.2$ K, while G_0 and K_g depend on the regime of crystallization for a given brand of iPP. K_g is inversely proportionally to the entropy of fusion, $\Delta s_f = \Delta h_f / T_m^0$, where Δh_f denotes the enthalpy of fusion. The negative pressure lowers the transitions temperatures. In the temperature range in which the iPP samples were crystallized, the reduction of undercooling, $T_m^0 - T_c$, is decisive; hence, the growth rate decreases upon the action of negative pressure. Then, it is possible to determine the depression of the equilibrium melting temperature, ΔT_m^0, from the ratio of the growth rate under negative pressure, G_p, to the growth rate at atmospheric pressure, G_i, that is, the initial growth rate before a weak spot formation:

$$\Delta T_m^0 = T_m^0 - T_c - \{(T_m^0 - T_c)^{-1} + T_c K_g^{-1} \ln(G_i/G_p)\}^{-1} \quad (2)$$

where T_m^0 is taken at atmospheric pressure. By knowing ΔT_m^0 and extrapolating the value of dT_m^0/dp [0.338 K/MPa (ref. 15), 0.38 K/MPa (ref. 16)] to the negative pressure range, one can calculate the negative pressure inside a weak spot.

The possible error made in the determination of the ΔT_m^0 value by neglecting the T_∞ dependence on the negative pressure was estimated in the following way: The new value, T'_∞, was evaluated as $T_\infty - \Delta T_\infty$, where ΔT_∞ equals the product of pressure and dT_g/dp, which is near 0.2 K/MPa for most polymers. Then, the new value, $\Delta T_m^{0\prime}$, was

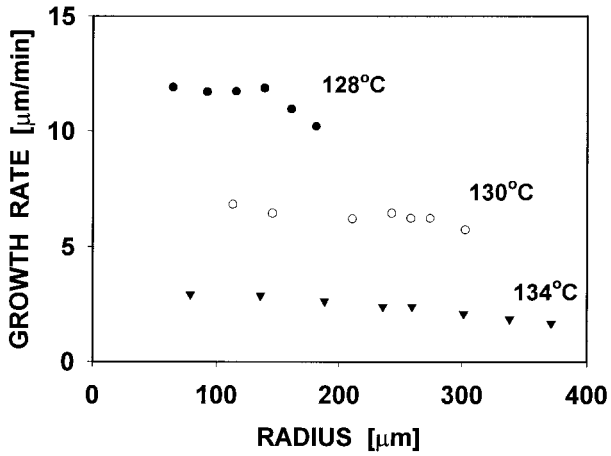

Figure 11 Dependencies of spherulite growth rate on radius of single isolated spherulites.

obtained by combination of the two formulas for the growth-rate dependence on T_c: the first one for the growth rate at atmospheric pressure and the second one for the growth rate under negative pressure, with T_∞ and T_m^0 being substituted by T'_∞ and $T_m^0 - \Delta T_m^{0\prime}$, respectively. It was found that the new values of $\Delta T_m^{0\prime}$ are higher only by a few percents.

In the present study, the values of K_g were determined on the basis of the plot

$\ln G + U[R(T_\infty - T_c)]^{-1}$ on $[T_c(T_m^0 - T_c)]^{-1}$: 1.47×10^5 K^2 in Regime II and 3.30×10^5 K^2 in Regime III. The Regime III $\rightarrow$ Regime II transition in iPP used in this study is near 136°C.[8]

The dependence of G on the spherulite radius, R, is shown in Figure 11 for isolated spherulites at T_c = 128, 130, and 136°C. At 128°C, G is nearly constant for R shorter than 100 μm but decreases for larger R. At higher T_c, the decrease of G with R is also seen. This indicates the fractionation of low molecular weight and atactic fractions during crystallization, depending on the T_c and on R. We also observed that at $T_c < 130$°C the spherulite growth rate inside weak spots after cavitation, G_{ac}, assumed usually its initial value, G_i, that is, before the weak spot formation, while at $T_c > 130$°C, G_{ac} was often lower than was G_i. It should be mentioned here that we excluded the residual negative pressure as the reason for the lower growth rate after cavitation. The pressure due to the surface tension q tending to collapse a bubble of radius r in a liquid is equal $2\ q/r$. To stabilize the bubble in a liquid, the negative pressure of the same value is necessary. For the bubble of radius 1 μm, the negative pressure in a polymer melt has to be near 0.03 MPa, which is far too small to have a noticeable effect on the spherulite growth rate. A collapse of a bubble, occasionally seen, could be caused by its insufficient size for a stable cavity at a decreased negative pressure.

It was suggested earlier[6] that the negative pressure inside a weak spot should depend on the momentary volume deficiency—hence, on the progression of crystallization inside a weak spot, $1 - S/S_i$, where S is the uncrystallized area in a weak spot, and S_i, the initial area of the melt confined in a weak spot. Since the depression of the spherulite growth rate G_p/G_i is a useful measure of negative pressure at isothermal conditions, the plot of G_p/G_i versus S/S_i should show how the negative pressure buildup depends on the sizes of the weak spots and the temperature of crystallization. In Figure 12, such a plot is shown for a series of weak spots differing in their sizes from 0.002 to 0.04 mm^2 during their crystallization at 130°C. In each weak spot, the growth rate lowers with the progression of crystallization, indicating the buildup of negative pressure. However, for smaller weak spots, the decrease of G_p/G_i with the decrease of S/S_i is initially slower and these weak spots do not cavitate, while for the largest weak spot, the growth rate decreases faster and the largest weak spot cavitates. In Figure 12(a), the growth rates, G_c, are also marked, at which cavitation occurred for other weak spots with sizes in the range 0.016–0.078 mm^2. The pressure at which the cavitation occurs varies although G_c/G_i at the moment of cavitation conforms to the dependence of G_p/G_i versus S/S_i inside the weak spots. No direct correlation of the negative pressure at the moment of cavitation can be found with any controlled parameter; probably, the cavities are nucleated on some impurities or heterogeneities present in the polymer melt. After cavitation, the growth rate abruptly increases, which is marked by arrows in Figure 12(a). For a higher crystallization temperature, the decrease of the growth rate inside the weak spots is slower even for a relatively large weak spot, as can be seen in Figure 12(a), where the respective curve is plotted with a dashed line for a 0.14-mm^2 cavitating weak spot crystallized at 134°C. In Figure 12(b), the respective values of ΔT_m^0 calculated from Figure 12(a) using eq. (2) are plotted against S/S_i. It is seen that ΔT_m^0 can reach 4 K for large weak spots with delayed cavitation.

In Figure 13, S/S_i at the moment of cavitation is plotted against the size of a weak spot for all

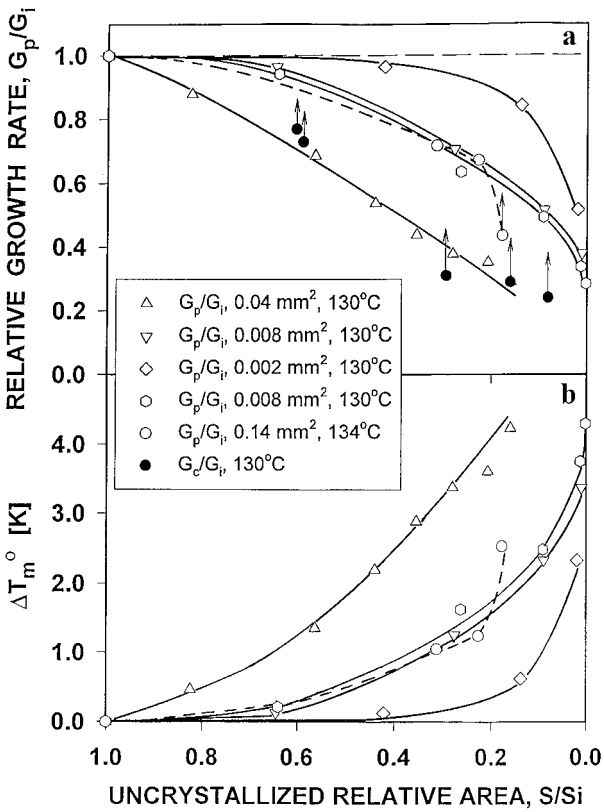

Figure 12 (a) Relative growth rate of iPP spherulites under negative pressure in weak spots and (b) the respective depression of equilibrium melting temperature, ΔT_m^0, calculated according to eq. (2) versus decreasing relative uncrystallized area S/S_i inside weak spots. Open symbols denote the values of G_p/G_i measured in weak spots until cavitation or in absence of cavitation, until the end of crystallization. Filled symbols denote the values measured right before the cavitation and also for other cavitating weak spots.

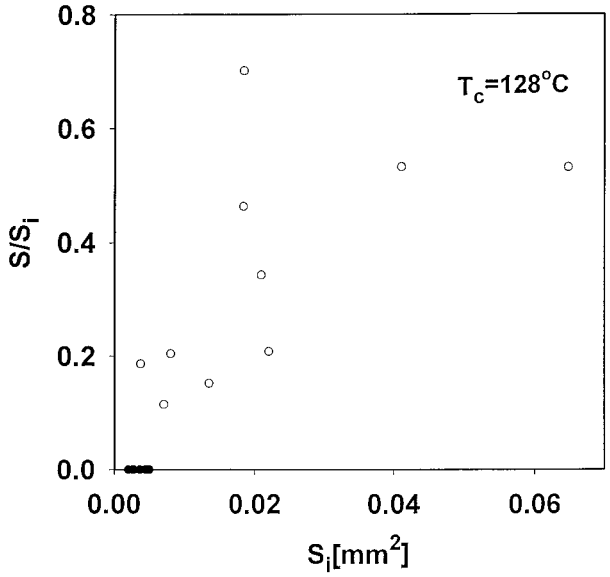

Figure 13 (Open symbols) Relative uncrystallized areas of weak spots, S/S_i, at the moment of cavitation during crystallization at 128°C plotted against their initial sizes S_i. The initial sizes of noncavitating weak spots marked by filled symbols for comparison.

cavitating weak spots from a fragment of a sample crystallized at 128°C. The sizes of the noncavitating weak spots found in that fragment of a sample are also marked in Figure 13 for comparison. It follows from the figure that larger weak spots tend to cavitate earlier.

In Figure 14, the depression of the equilibrium melting temperature, ΔT_m^0, is plotted versus T_c, where ΔT_m^0 was calculated according to eq. (2) from the ratios G_c/G_i and also from G_c/G_{ac} for $T_c > 130$°C. The highest value of ΔT_m^0, 5.9 K, was obtained for $T_c = 126$°C. It corresponds to the negative pressure value of 15.5 or 17.5 MPa, depending on assumed dT_m^0/dT value of 0.38 K/MPa (ref. 15) or 0.338 K/MPa (ref. 16), respectively. In spite of the data scatter, the tendency of the decrease of ΔT_m^0 and, hence, also the negative pressure value, with increasing T_c is visible, especially if G_{ac} is taken as growth-rate value at atmospheric pressure. This relationship is similar to the dependence of ΔT_m^0 on T_c obtained from the

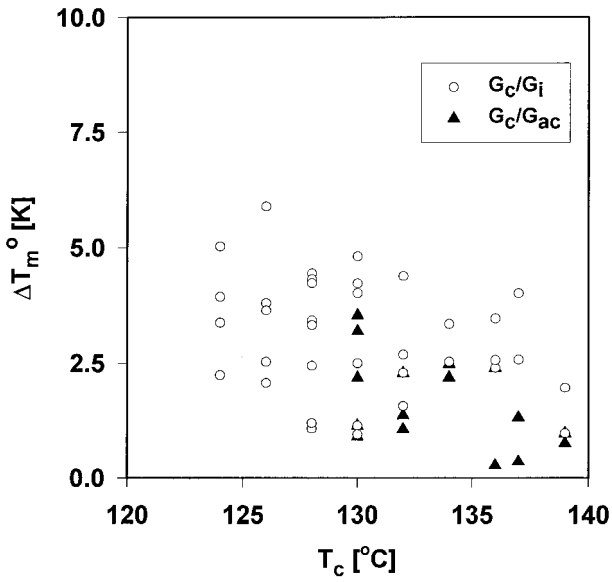

Figure 14 Depression of equilibrium melting temperature, ΔT_m^0, in weak spots in iPP thin film between microscopic glasses calculated according to eq. (2) from G_c/G_i ratios versus crystallization temperature, T_c.

measurements of the melting temperature increase in the weak spots; however, the maximum values determined from the growth rate are larger for higher crystallization temperatures.

DISCUSSION AND CONCLUSIONS

From the measurements of the spherulite growth rate in the weak spots at 130°C, it follows that the pressure buildup with decrease of the relative uncrystallized volume in the smaller weak spots is initially slower than in the larger ones. This could be explained by the partial relaxation of stresses, probably by displacement of the amorphous phase in the surrounding spherulites. Since volume deficiency, which is the reason for negative pressure development, depends on the ratio of noncrystallized area to the initial area of a weak spot, while the ability to relax stresses is related to a weak spot circumference; hence, one can expect more efficient stress relaxation in smaller weak spots. While small weak spots do not cavitate, the larger ones cavitate at various levels of negative pressure. However, G_c/G_i, at the moment of cavitation, conforms to the dependence of G_p/G_i versus the progression of crystallization inside the weak spots. This indicates that in large weak spots the relaxation of stresses is less effective and the negative pressure buildup is governed by an increasing volume deficiency. The cavitation at different levels of negative pressure points out the heterogeneous nucleation mechanism similarly as in low molecular weight liquids, for example, water, where cavitation nuclei are believed to be solid hydrophobic particles with crevices filled with air [e.g., ref. 17]. The larger weak spots tend to cavitate at a lower negative pressure, which results from the increased probability of the presence of a cavitation nucleus inside a confined melt. The reduction of this probability with decrease of the weak spot size, together with the initially slower negative pressure buildup with the progression of crystallization, prevents cavitation in the smallest weak spots. The negative pressure buildup with the progression of crystallization in a large cavitating weak spot at 134°C is slower than in the cavitating weak spots at 130°C. The slower increase of the negative pressure at a higher crystallization temperature results in less frequent cavitation although the weak spots as well as spherulites are larger. The slower negative pressure buildup can be explained as the result of its more effective relaxation by displacement of the polymer in the surrounding spherulites due to slower spherulite growth, lower viscosity, a coarser spherulitic structure, reduced cross-hatching, and weaker bonding between the crystalline and amorphous phases.

The cavitation at the spherulites–melt interphase could be a secondary effect resulting from the superposition of negative pressure and an acoustic wave produced by the primary cavitation event. This suggestion is also supported by the observation of simultaneous cavitation of neighboring weak spots, well visible at a lower crystallization temperature.

It was observed in the past that the mechanically induced negative pressure wave causes cavitation during crystal growth in supercooled organic liquids while no cavitation was observed in the same liquid during the melting of crystals.[18] The observation was attributed to the ability of the solid–liquid interphase to nucleate cavitation during crystallization. SEM studies have shown that small cavitation bubbles arranged in rows are embedded in the polymer beneath the sample surface. The results of atomic force microscopy of these voids described in ref. 5 demonstrated that the voids do not open to the sample surface. From light microscopy observation, it follows that they are located at the crystallization front where it adheres to the glass at the moment of cavitation, so their appearance is influenced by the polymer contact with the glass. The changes in the cavitation pattern visible with increase of the crystallization temperature could be attributed to alterations of the morphology of the crystallization front.

The cavitation along the spherulite boundaries and radii occurring at higher crystallization temperatures simultaneously with cavitation inside the weak spots indicates the presence of a molten polymer there. This is most probably the result of fractionation during crystallization which is enhanced by the negative pressure buildup, reducing supercooling in the weak spots. The fractionation is responsible for the incomplete growth rate recovery after cavitation observed at higher crystallization temperatures. The fractionation leads to an increasing concentration of low molecular weight and atactic polymer fractions in front of the growing spherulite. Finally, these fractions, having a lower ability or that are unable to crystallize, are entrapped along interspherulitic boundaries and between lamellas in the spherulite peripheries and cavitate when subjected to

negative pressure as does the melt inside the weak spots. The cavitation along the spherulite boundaries and radii occurring upon cooling in the weak spots which did not cavitate during isothermal crystallization results from increase of the negative pressure due to crystallization of the melt rich with low molecular weight and atactic polymer fractions.

The nucleation of spherulites on cavitational bubbles was investigated and discussed by Varga and Ehrenstein.[11] However, the additional mechanism promoting primary nucleation of spherulites after negative pressure release is also possible, which especially concerns α spherulites without voids visible in the centers. This is so-called athermal nucleation,[19] meaning that unstable embryos in the melt become the nuclei of spherulites because of an abrupt reduction of critical nucleus sizes due to a rapid increase of supercooling.

The negative pressure determined at the moment of cavitation decreases with increase of the crystallization temperature. A similar tendency was observed earlier in refs. 7 and 8, where the negative pressure in iPP was estimated using measurements of elevation of the melting temperature in the weak spots. However, the growth-rate measurements allowed one to determine the negative pressure also below 130°C, that is, where no elevation of the melting temperature due to increased lamella thickness was previously observed. It should be mentioned that in the past the decrease of negative pressure causing cavitation of low molecular weight liquids with the temperature was observed in a broad temperature range.[20, 21]

The results of this research point out the activity of a heterogeneous nucleation mechanism of cavitation in polymer melts—hence, depending to a large extent on the polymer purity. The other important observation is the role of weak spot sizes connected to spherulite sizes: By decreasing the sizes of the spherulites and, hence, the weak spots, it is possible to suppress cavitation inside the weak spots during spherulite growth. However, if the crystallization temperature is too high, this may lead to cavitation along interspherulitic boundaries after formation of the spherulitic structure, which is also unfavorable for the strength of material. Those effects are particularly important for solidification of thick wall products crystallizing at high temperature due to slow heat dissipation.

This research was supported primarily by the State Committee for Scientific Research, Poland, through the Centre of Molecular and Macromolecular Studies, PAS, under Grant 7 T08E 016 12.

REFERENCES

1. Galeski, A.; Piorkowska, E. J Polym Sci Polym Phys Ed 1983, 21, 1313.
2. Galeski, A.; Piorkowska, E. J Polym Sci Polym Phys Ed 1983, 21, 1323.
3. Monasse, B.; Haudin, J. M. Coll Polym Sci 1985, 263, 822.
4. Monasse B.; Haudin, J. M. Coll Polym Sci 1988, 266, 679.
5. Thoman, R.; Wang, Ch.; Kressler, J.; Mulhaupt, R. Macromol Chem Phys 1996, 197, 1085.
6. Pawlak, A.; Galeski, A. J Polym Sci Part B Polym Phys 1990, 28, 1813.
7. Piorkowska, E.; Galeski, A. J Polym Sci Part B Polym Phys 1993, 31, 1285.
8. Pawlak, A.; Piorkowska, E. J Appl Polym Sci 1999, 74, 1380.
9. Olley, R. H.; Basset D. C., poster on Polymer Physics, Bristol, UK, April 1991.
10. Zadlo, A. M.Sc. Thesis, CMMS, Polish Academy of Sciences, 1986.
11. Varga, J.; Ehrenstein, G. W. Polymer 1996, 37, 5959.
12. Galeski, A.; Koenczoel, L.; Piorkowska, E.; Baer, E. Nature 1986, 325, 40.
13. Galeski, A.; Piorkowska, E.; Koenczoel, L.; Baer, E. J Polym Sci Part B Polym Phys 1990, 28, 1171.
14. Clark, E. J.; Hoffman, J. D. Macromolecules 1984, 17, 878.
15. Karl, V.; Asmussen, F.; Uberreiter, K. Makromol Chem 1977, 178, 2037.
16. Leute, U.; Dolhopf, W.; Liska, E. Coll Polym Sci 1978, 256, 914.
17. Holl, J. W. In Cavitation State of Knowledge; ASME, New York, 1969; p 26.
18. Pease, D. C.; Blinks, R. L. J Phys Chem 1947, 51, 556.
19. Ziabicki, A.; Alfonso, C. G. Coll Polym Sci 1994, 272, 1027.
20. Briggs, L. J. J Appl Phys 1950, 7, 721.
21. Briggs, L. J. J Chem Phys 1951, 19, 970.